Journal of Materials Chemistry A

RSC Publishing

PAPER

View Article Online
View Journal | View Issue

Cite this: J. Mater. Chem. A, 2013, 1, 7332

Electrospinning lead-free $0.5Ba(Zr_{0.2}Ti_{0.8})O_3$–$0.5(Ba_{0.7}Ca_{0.3})TiO_3$ nanowires and their application in energy harvesting†

Weiwei Wu,[a] Li Cheng,[a] Suo Bai,[a] Wei Dou,[a] Qi Xu,[a] Zhiyang Wei[a] and Yong Qin*[ab]

Received 24th February 2013
Accepted 3rd April 2013

DOI: 10.1039/c3ta10792b

www.rsc.org/MaterialsA

High performance nanogenerators (NGs) are critically important for energy harvesting and powering micro/nano-devices. Environmentally friendly nanowires (NWs) with high piezoelectric coefficients are highly desirable for enhancing NGs' performance and expanding their applications. In this paper, we synthesized a new kind of lead-free $0.5Ba(Zr_{0.2}Ti_{0.8})O_3$–$0.5(Ba_{0.7}Ca_{0.3})TiO_3$ (BZT–BCT) NWs with high piezoelectric coefficients through the electrospinning method and subsequent calcining process. Their crystal structure and formation mechanism were systematically studied. Furthermore, BZT–BCT NWs were made into a high performance flexible NG. It could harvest weak mechanical movement energy and generate an output voltage of 3.25 V and output current of 55 nA, which is large enough to directly power a commercial liquid crystal display (LCD).

1 Introduction

As the building blocks of transducers,[1] NGs,[2] piezoelectric sensors,[3] actuators,[4] and ferroelectric nonvolatile memory and transistor devices,[5] piezoelectric materials have been extensively investigated.[6] In previous reports, benefiting from their excellent piezoelectric properties, lead oxide based ferroelectrics, especially lead zirconate titanate (PZT), have been the most widely used piezoelectric materials.[6] However, pollution because of PbO's evaporation during the sintering process has greatly hindered the applications of Pb-based ferroelectric materials; even in 2003, the European Union (EU) included PZT as a hazardous substance in its legislature to be substituted by safe materials.[7] Therefore, developing a lead free and environmentally friendly material with a piezoelectric coefficient comparable to that of PZT (200–710 pC N^{-1})[6,8] is highly desirable for high performance NGs and their applications.[8–10]

A representative feature of a material with high piezoelectric performance is the existence of a morphotropic phase boundary (MPB).[11–14] Due to the placing of the composition of the material in the proximity of a composition-induced phase transition between two ferroelectric phases, a larger piezoelectric coefficient has usually been obtained in ferroelectric materials with MPB.[15–19] Recently, many kinds of lead-free MPB based piezoelectric ceramics have been explored and studied, such as $(K,Na)NbO_3$ (KNN),[20,21] $(K,Na)NbO_3$–$LiTaO_3$ (KNN–LT),[22] $(K,Bi)TiO_3$–$BaTiO_3$ (KBT–BT),[23] $(Na_{0.5}Bi_{0.5})TiO_3$–$(K_{0.5}Bi_{0.5})TiO_3$–$BaTiO_3$ (NBT–KBT–BT)[24] and BZT–BCT.[25] Among these materials, $0.5Ba(Zr_{0.2}Ti_{0.8})O_3$–$0.5(Ba_{0.7}Ca_{0.3})TiO_3$ is a kind of BZT–BCT material with a MPB and has attracted much research interest due to its high piezoelectric coefficient (620 pC N^{-1}).[25–29] In previous reports, a solid state reaction, the Czochralski method and the sol–gel method have been utilized to synthesize BZT–BCT powder, bulk single crystals and submicron particles.[25,27,28]

Since its invention in 2006,[2] NGs have become a potential power source for portable, personal and wearable self-powered nano/micro systems. Compared with traditional piezoelectric cantilevers, NGs can harvest irregular weak mechanical movement over a wide frequency range, which requires piezoelectric materials to work under different conditions.[30–33] For high performance NGs, piezoelectric NWs are desirable due to their high flexibility and strain tolerance.[34–36] Upon further considering the efficiency of electromechanical conversion and environmental friendliness, lead-free NWs with high piezoelectric coefficients should be most desirable. So BZT–BCT NWs are perfect candidates for NGs. But due to their complicated composition and symmetry structure, they are difficult to synthesize *via* conventional approaches such as CVD and the hydrothermal method.[37] Currently, the synthesis of BZT–BCT NWs and the corresponding textiles consisting of well aligned NWs still presents challenges. Thus, exploring a simple, low cost and highly efficient method to prepare BZT–BCT NWs is of great value for the development of NGs and energy harvesting.

In this study, we successfully synthesized a textile composed of well aligned lead-free BZT–BCT NWs parallel with each other through an electrospinning method and a subsequent sintering

[a]Institute of Nanoscience and Nanotechnology, Lanzhou University, Lanzhou 730000, China. E-mail: qinyong@lzu.edu.cn; Fax: +8609318915038; Tel: +8609318915038
[b]Beijing Institute of Nanoenergy and Nanosystems, Chinese Academy of Sciences, Beijing 100085, China

† Electronic supplementary information (ESI) available. See DOI: 10.1039/c3ta10792b

process. Their perovskite structure was confirmed by X-ray diffraction (XRD), selected area electron diffraction (SAED), convergent beam electron diffraction (CBED), and Raman spectroscopy. The elements and their distributions were characterized by energy dispersive X-ray spectroscopy (EDS) and EDS mapping. Their formation mechanism was studied, and they were made into a flexible NG to study their energy harvesting properties for weak mechanical movement. The NGs successfully translated mechanical energy into electricity and gave a peak output voltage of 3.25 V and a peak output current of 55 nA. A commercial LCD was directly powered by the BZT–BCT textile NG.

2 Experiments and methods

2.1 Synthesis of 0.5BZT–0.5BCT NWs

All the solvents and raw materials were analytically pure and used without any further purification. The flow chart in Fig. 1 shows the process of preparing the precursor for electrospinning. First, 3.000 g of ethanol, 1.500 g of acetylacetone and 9.500 g of acetic acid were added into a 25 ml Erlenmeyer flask and mixed. Then, 2.475 g of tetrabutyl titanate, 2.172 g of barium hydroxide, 0.090 g of calcium hydroxide and 0.394 g of zirconium acetylacetonate were added into the above solution in sequence. After stirring for more than 24 hours, 0.525 g of polyvinylpyrrolidone (PVP) (M_w = 1 300 000) was dissolved into the solution to form a transparent precursor with a suitable viscosity. Later, the precursor was electrospun into NWs under a high voltage of 30 kV with a spinning rate of 0.1 ml min^{-1}. The distance between the needle tip and the collector was about 25 cm. During the electrospinning process, the temperature and humidity were about 20 °C and 30%, respectively. The BZT–BCT NWs were collected by a collector consisting of suspended parallel electrodes to form a textile composed of laterally aligned NWs.[34] Then the textile was peeled off from the collector and laid on a flat corundum substrate. Finally, the textile was sintered at 700 °C for 3 hours at a ramp rate of 2 °C per minute.

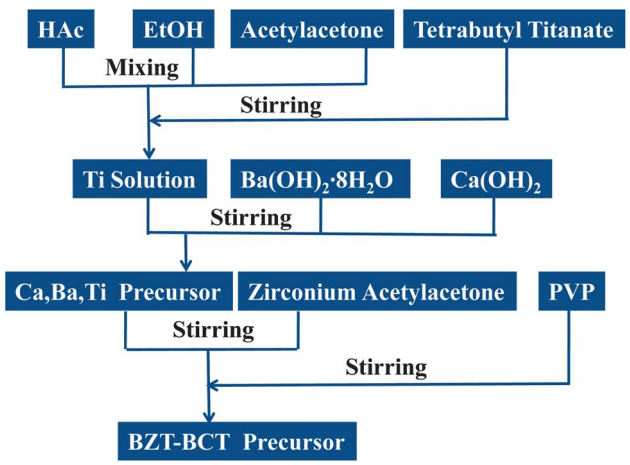

Fig. 1 Flow chart for the preparation of the precursor of BZT–BCT NWs.

2.2 Fabrication of the flexible nanogenerator based on BZT–BCT NWs

The NG based on BZT–BCT NWs was fabricated as in a previous report.[34] First, a piece of poly(ethylene terephthalate) (PET) film was cleaned using acetone, ethanol and deionized water, in sequence. Subsequently, polydimethylsiloxane (PDMS) was spin coated on the dry PET film at 5000 revolutions per minute (rpm) for 1 minute to make an ultrathin PDMS layer. Then, this substrate was precured at 70 °C for 10 minutes. Then, a small piece of BZT–BCT textile composed of aligned NWs was attached tightly to the substrate. Later, Ag electrodes were deposited at two ends of the NWs using a shadow mask and magnetron sputtering. The electrodes were connected with copper wires by silver paste. Finally, this device was packaged with PDMS. After poling with a 1.5 kV mm^{-1} electric field at 90 °C for 2 hours, the device was cooled down to room temperature using a field cooling method.[38]

2.3 Characterization of the NG's output

For the characterization of NG's performance, one end was fixed to a holder, and the other end was pushed back and forth using a linear motor (Linmot E1100) to stretch and release the NWs to generate electricity. The output signals of the NG were characterized using preamplifiers (Stanford Research System SR560 and SR570).

3 Results and discussions

3.1 Morphology and structure of BZT–BCT NWs

Fig. 2a is a representative scanning electron microscopy (SEM) image of BZT–BCT NWs. They have a relatively uniform diameter of ~175 nm. Meanwhile, the surface of the sintered NWs is not quite smooth because of grain growth at high temperature, which can also be seen in Fig. 2b. Those NWs are composed of small BZT–BCT nanoparticles stacked together. From the transmission electron microscopy (TEM) image shown in Fig. 2b, we can see that the NWs are compact and continuous. The crystal lattice spacings marked in the inset of Fig. 2b are 0.30 nm and 0.20 nm, which correspond to (011) and (211) crystal planes of a quasi tetragonal structure, respectively. Meanwhile, the regular atomic arrangement indicates that the synthesized BZT–BCT NWs have good crystallinity. Fig. 2c shows a SAED pattern which indexes to a perovskite structure. The single crystal diffraction patterns were characterized by the CBED method. As shown in Fig. 2d, the lattice spacings along the [100], [001] and [101] orientations are about 0.40 nm, 0.42 nm and 0.30 nm, respectively. Here, the value of "c/a" is about 1.05 which is a little larger than that in a previous report.[25] The lattice spacing along [111] direction is measured as 0.25 nm in Fig. 2e. Similarly, the lattice spacing along [211] direction is 0.20 nm as shown in Fig. 2f. The distance of these different crystal planes and the angle of about 88° between the (100) and (001) crystal planes prove that the unit cell is a quasi tetragonal structure.

Furthermore, EDS and scanning transmission electron microscopy (STEM) mapping were used to study the element

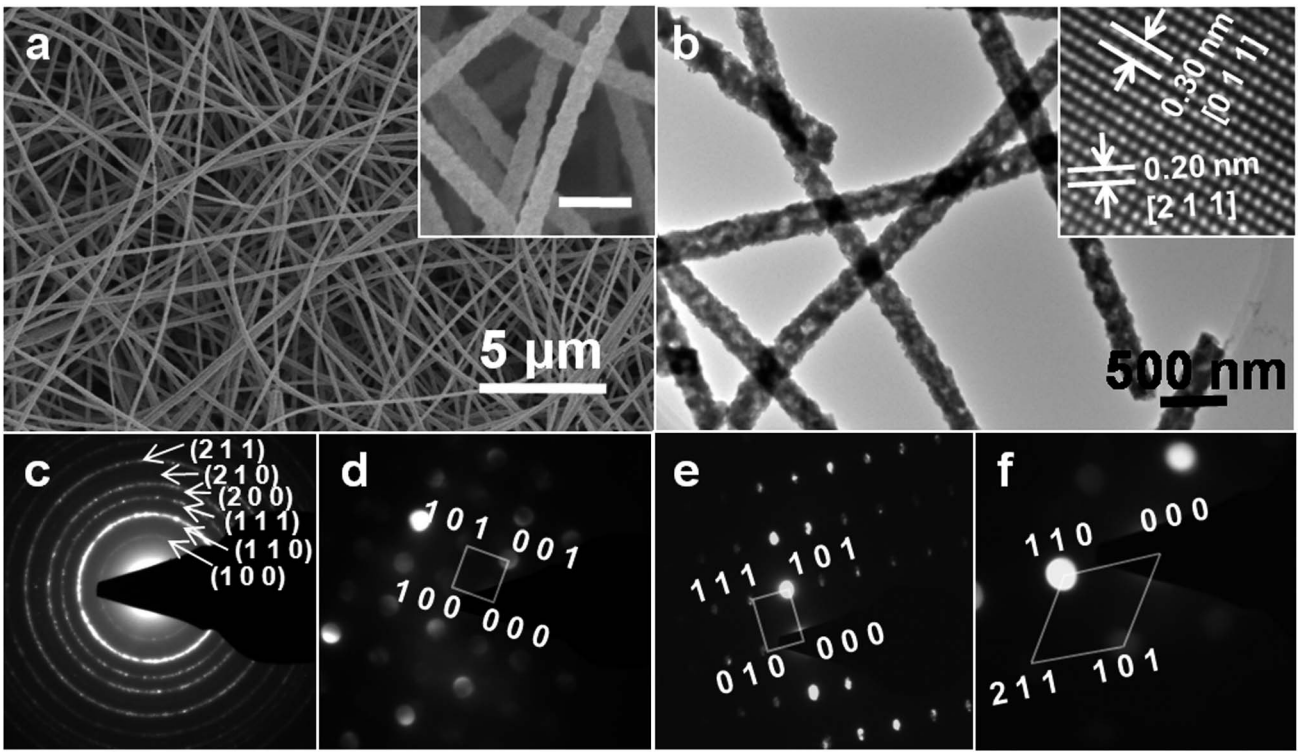

Fig. 2 (a) Low magnification SEM image of sintered BZT–BCT NWs. The inset is a high magnification SEM image. The scale bar is 500 nm. (b) TEM image of BZT–BCT NWs. The inset is the HRTEM image. (c) SAED pattern of BZT–BCT NWs. (d–f) The CBED pattern of BZT–BCT NWs.

distribution in the NWs. Fig. 3a is a typical EDS pattern obtained from the area in Fig. 2a. All the elements in BZT–BCT were detected, and the measured atomic percentages of barium, calcium, titanium, zirconium and oxygen (Table 1) are consistent with the stoichiometric ratio of BZT–BCT. Fig. 3b is a typical STEM image of two BZT–BCT NWs characterized by a high angle annular dark-field imaging (HAADF) detector. Fig. 3c–g show that all the chemical elements of BZT–BCT are distributed homogeneously throughout the NWs.

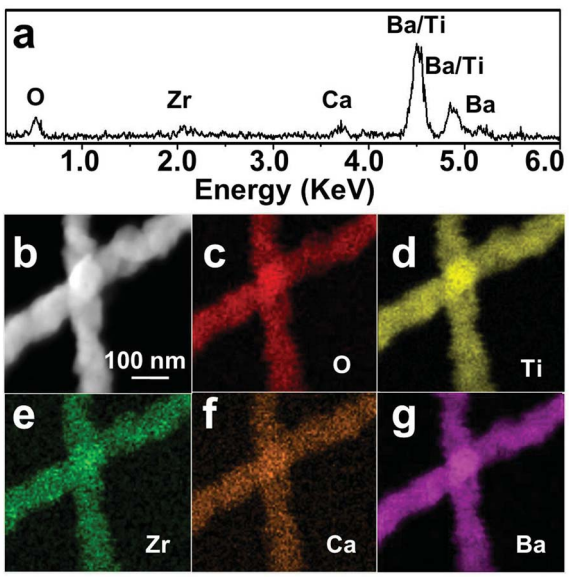

Fig. 3 (a) EDS of BZT–BCT NWs. (b) STEM image of BZT–BCT NWs. (c–g) EDX mapping images of different chemical elements.

Fig. 4a is the XRD pattern of the BZT–BCT NWs, which can be indexed to the polycrystalline perovskite structure. The diffraction peaks broaden obviously due to the small BZT–BCT particles made up of NWs, which mask the peak splitting caused by tetragonality (c/a). But the Raman spectrum and analysis (Fig. 4b and Table 2) reveals that Zr and Ca atoms have come into the crystal cell to form BZT–BCT.[28,39] Therefore, we reconstructed the unit cell of BZT–BCT by modifying the unit cell of $BaTiO_3$ (BTO) (the inset of Fig. 4d). For BTO, "A" sites are occupied by Ba atoms, "B" sites are occupied by Ti atoms, and O atoms are located at the face centers to form oxygen octahedra. BZT–BCT can be regarded as BTO doped with Zr and Ca atoms. The Ca and Zr atoms partly replace the existing atoms at the "A" and "B" sites, respectively, forming a non-Pb pseudo binary piezoelectric system.[40,41]

Table 1 The EDS analysis of BZT–BCT nanofibers

Element	Theoretical atomic%	Measured atomic%
Ba	42.5	42.36
Ca	7.5	7.38
Ti	45.0	45.46
Zr	5.0	4.8

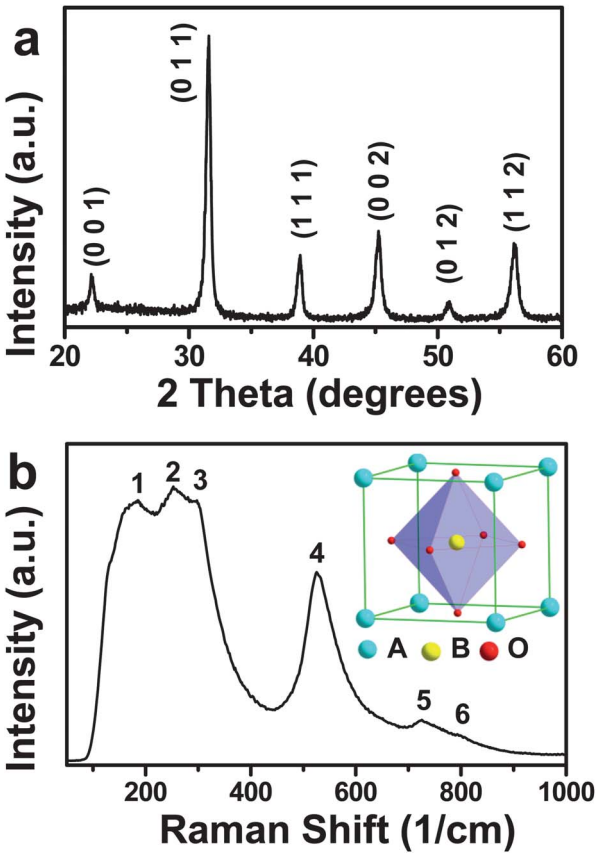

Fig. 4 (a) XRD pattern of BZT–BCT NWs. (b) Raman spectrum of BZT–BCT NWs. The inset is a schematic image of the BTO unit cell.

Table 2 Room-temperature Raman mode assignments in the BZT–BCT

Number	Raman shift (cm^{-1})	Symmetry	Reference
1	186	A_1 (TO)	39
2	252	A_1 (TO)	28
3	298	B_1, E (TO + LO)	28
4	525	A_1, E (TO)	28
5	725	A_1, E (LO)	28
6	800	A_{1g}	39

3.2 The formation mechanism of BZT–BCT NWs

The sintering temperature for forming pure phase BZT–BCT NWs was 700 °C, which is much lower than the 1450 °C in the solid phase reaction method.[25] Clarifying the formation mechanism of BZT–BCT at such a low temperature is extremely important for the synthesis of this kind of lead free material. To make the mechanism clear, further characterization was used to explore the whole preparation process of BZT–BCT NWs. The fast Fourier transform infrared spectra (FTIR) of as-spun NWs (Fig. 5a) shows that they are made up of organometallic compounds and residual solvent. The reaction process was studied through the curves of thermogravimetric analysis (TGA) and differential thermal analysis (DTA) (Fig. 5b). In period "I", the absorption of heat and weight loss can be ascribed to solvent evaporation. When the temperature rises to period "II", a sharp peak for the DTA and a large weight loss are observed. After 3 hours of calcining at 440 °C, all the characteristic peaks in the FTIR spectra corresponding to the organic functional groups have disappeared, which means that the organics have decomposed. This is also displayed by the photograph in Fig. 5d; the film made with NWs becomes black due to the organic decomposition. Meanwhile, the XRD pattern only shows a broad amorphous peak (Fig. S1†). Thus, in period "II", PVP is decomposed into amorphous carbon, and meanwhile, other raw materials are decomposed into corresponding amorphous inorganics. As the temperature increases to 580 °C (period "III"), the color of the NWs turns from black to white, accompanied by an endothermic peak and weight loss. This process corresponds to the burning of most of the carbon and the formation of inorganic nanocrystals. According to the XRD pattern in Fig. S2,† we can confirm that the intermediate compounds are BaO, TiO_2, ZrO_2, $BaTiO_3$ and $(Ba_{0.7}Ca_{0.3})TiO_3$ at this time. But some residual C still exists and will be totally burnt off at a higher temperature. When the temperature reaches 700 °C (period "IV"), pure phase BZT–BCT is obtained (shown in Fig. 5c). Furthermore, from Fig. 5c, no phase transformation is observed even upon sintering BZT–BCT NWs at 850 and 1000 °C in period "V". The only change is that the diffraction peaks become narrower, which can be ascribed to an increase of the crystal size with an increase of the annealing temperature (Table 3).

According to the above analysis, a possible formation mechanism of BZT–BCT is proposed in the schematic diagrams as shown in Fig. 5e. It starts with a bright yellow transparent precursor that contains solvent, PVP, tetrabutyl titanate ($C_{16}H_{36}O_4Ti$), zirconium acetylacetone ($Zr(C_5H_7O_2)_4$), calcium acetate ($Ca(CH_3COO)_2$) and barium acetate ($Ba(CH_3COO)_2$). As the calcinating temperature increases, the following phenomena and reactions occur in sequence.

Room temperature to 440 °C: solvent evaporates.

$$PVP \rightarrow C$$

$$Ba(CH_3COO)_2 + 4O_2 = BaO + 4CO_2 + 3H_2O$$

$$Ca(CH_3COO)_2 + 4O_2 = CaO + 4CO_2 + 3H_2O$$

$$2Zr(C_5H_7O_2)_4 + (46 + x)O_2 = 2ZrO_x + 40CO_2 + 28H_2O$$

$$2C_{16}H_{36}O_4Ti + (46 + x)O_2 = 2TiO_x + 32CO_2 + 36H_2O$$

440–580 °C:

$$C + O_2 = CO_2$$

$$2TiO_x + (2 - x)O_2 = 2TiO_2$$

$$2ZrO_x + (2 - x)O_2 = 2ZrO_2$$

$$BaO + TiO_2 = BaTiO_3$$

$$7BaO + 3CaO + 10TiO_2 = 10(Ba_{0.7}Ca_{0.3})TiO_3$$

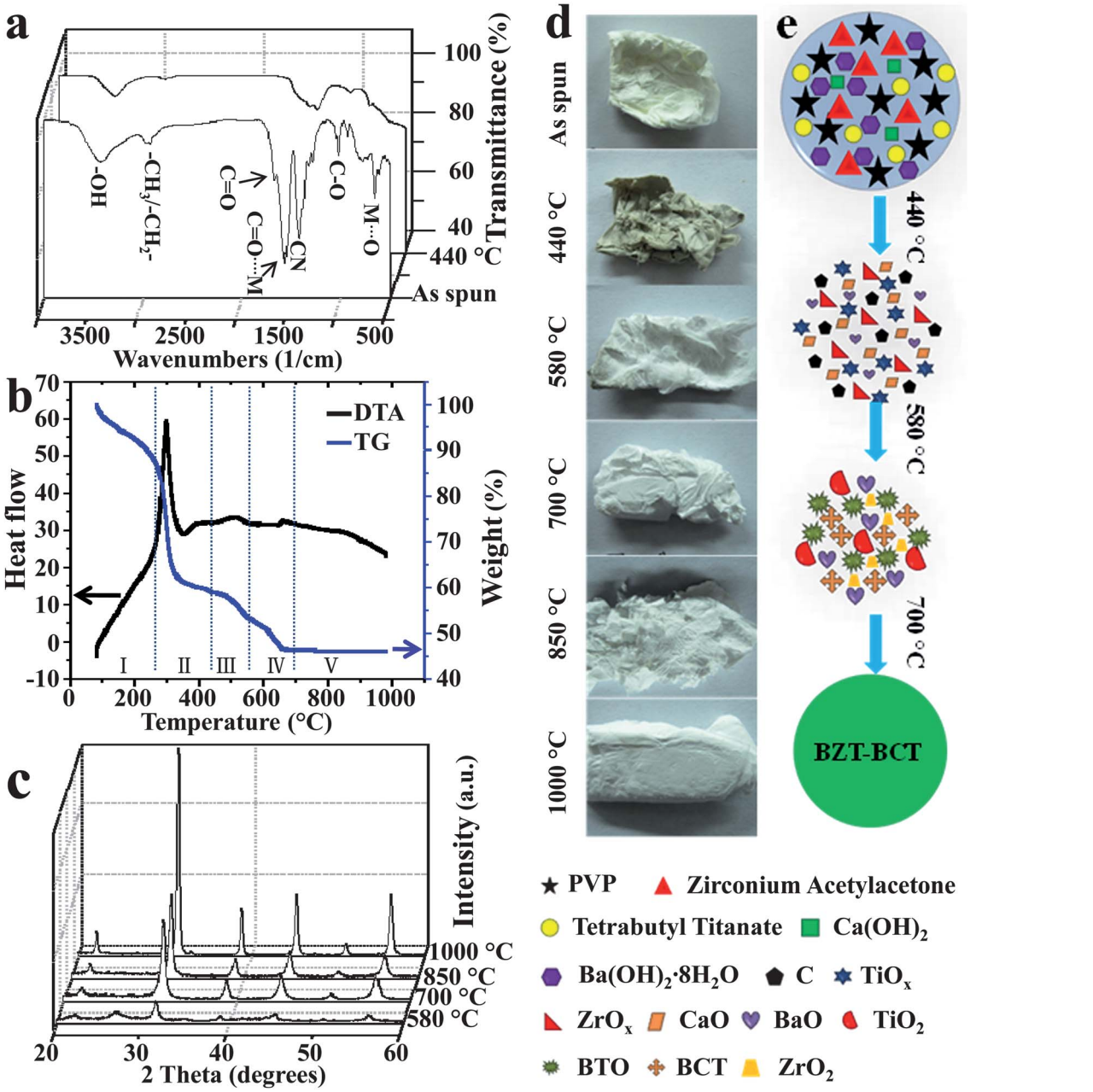

Fig. 5 (a) FTIR spectrum of as-spun NWs and those sintered at 440 °C. (b) TG and DTA curves. (c) XRD patterns of NWs sintered at different temperatures. (d) Photographs of NWs sintered at different temperatures. (e) Schematic diagrams of the formation process of BZT–BCT.

Table 3 Average crystallite sizes of the BZT–BCT

Temperature (°C)	Bragg's angle (°)	FWHM (rad)	Particle diameter (nm)
700	45.18	0.01108	17.56
850	45.24	0.00856	22.74
1000	45.21	0.00511	38.09

580–700 °C:

$$10BaO + 2ZrO_2 + 8TiO_2 = 10Ba(Zr_{0.2}Ti_{0.8})O_3$$

$$8BaTiO_3 + 2ZrO_2 + 2BaO = 10Ba(Zr_{0.2}Ti_{0.8})O_3$$

$$Ba(Zr_{0.2}Ti_{0.8})O_3 + (Ba_{0.7}Ca_{0.3})TiO_3 = 2[0.5Ba(Zr_{0.2}Ti_{0.8})O_3–0.5(Ba_{0.7}Ca_{0.3})TiO_3]$$

700–1000 °C:

0.5BZT–0.5BCT crystal grows.

In the above reaction, metal oxides obtained from the decomposition of organometallic compounds have a low reaction potential barrier to form "O" octahedra that are the framework of BZT–BCT unit cell. Meanwhile, the metal ions

fill the interspaces of the framework to form the initial nuclei for the BZT–BCT. In the following grain growth process, all materials are mixed at the molecular level, which enlarges the contact area and shortens the diffusion of ions greatly. So the energy barrier of ion diffusion is very low. Low energy barriers of nuclei formation and diffusion mean that the pure phase BZT–BCT NWs can be synthesized at low temperature of 700 °C.

3.3 BZT–BCT NWs based nanogenerator

To study the energy harvesting properties of the BZT–BCT NWs, they were electrospun into well aligned nanowires (Fig. S3†) and made into a flexible NG as shown in Fig. 6a according to the design of our previous work.[34] The 5 μm thick electrospinning textile composed of BZT–BCT NWs was adhered on a piece of PET film with a thickness of 200 μm using a thin layer of PDMS. Two strip-like electrodes were deposited on its two ends through magnetron sputtering. Then, they were packaged with soft PDMS to form a NG (shown in Fig. 6a). To obtain good piezoelectric properties, the field cooling method[38] was used to polarize the BZT–BCT NWs. A linear motor was used to periodically deform the thick PET film to stretch and release the NWs along the direction of their length. The open circuit voltage and short circuit current were measured to characterize the performance of the NG. From Fig. 6b and c, the maximum output voltage and current reached 3.25 V and 55 nA, respectively. The output power of the NG was calculated according to the following equation:[42]

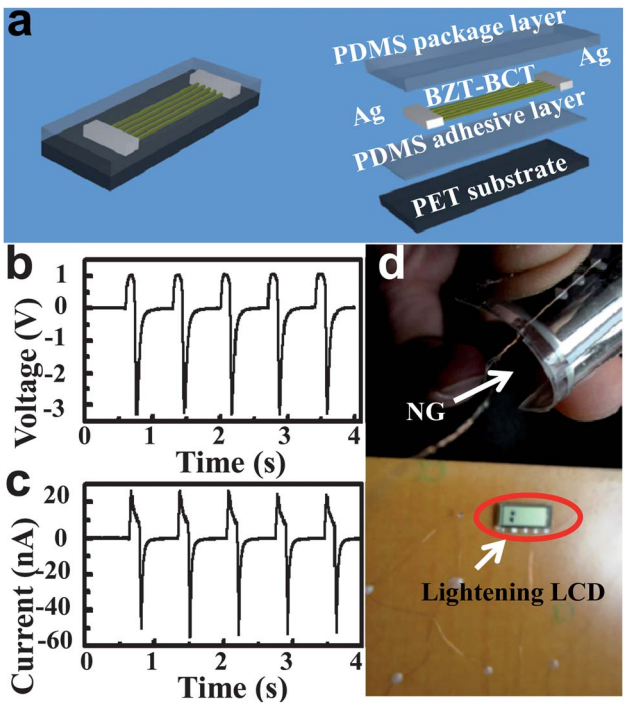

Fig. 6 (a) Schematic diagram of a NG. (b) Open circuit voltage output of the NG. (c) Short circuit current output of the NG. (d) Photograph of the NG powering a commercial LCD.

$$P_l = \frac{1}{T}\int \frac{U^2(t)}{R_l}\mathrm{d}t$$

where $U(t)$ is the real-time voltage, R_l is the impedance of the voltage preamplifier (100 MΩ), and T is the period of stretching and releasing which can be obtained from the measured output voltage (Fig. 6b). The measured output power reached 20.3 nW. The total volume of BZT–BCT textile was about 6×10^{-5} cm^3 (length 1.5 cm, width 0.8 mm and thickness 5 μm). Thus, the power density was 338 μW cm^{-3}. This output is large enough to directly power a commercial LCD (shown in Fig. 6d and the video, ESI†).

4 Conclusions

In summary, lead-free BZT–BCT NWs with a high piezoelectric coefficient and the corresponding textile were synthesized through the electrospinning method and post annealing process. Their crystal structure and formation mechanism were systematically studied. Metal oxides were obtained from the decomposition of organometallic compounds and sintered to further form perovskite BZT–BCT NWs at low temperature (700 °C). Furthermore, these BZT–BCT NWs were made into a flexible NG. Its output voltage, current and power density could reach 3.25 V, 55 nA and 338 μW cm^{-3} respectively, which are large enough to make a lighter commercial LCD.

Acknowledgements

Research was supported by Fok Ying Tung education foundation (131044), the Fundamental Research Funds for the Central Universities (no. lzujbky-2010-k01, lzujbky-2012-210), Special Talent Funding of Lanzhou University, and New Academic Researcher Award for Doctoral Candidates. We thank Dr Fang Niu for helping analyze the FTIR results. We also thank Dr Long Gu for help with preparing samples.

Notes and references

1 M. D. Ward and D. A. Buttry, *Science*, 1990, **249**, 1000.
2 Z. L. Wang and J. H. Song, *Science*, 2006, **312**, 242.
3 F. Patolsky, A. Lichtenstein and I. Willner, *Nat. Biotechnol.*, 2001, **19**, 253.
4 P. Muralt, *J. Micromech. Microeng.*, 2000, **10**, 136.
5 J. I. Sohn, S. S. Choi, S. M. Morris, J. S. Bendall, H. J. Coles, W.-K. Hong, G. Jo, T. Lee and M. E. Welland, *Nano Lett.*, 2010, **10**, 4316.
6 G. H. Haertling, *J. Am. Ceram. Soc.*, 1999, **82**, 797.
7 EU-Directive 2002/96/EC: Waste Electrical and Electronic Equipment (WEEE), *Off. J. Eur. Union*, 2003, **46**(L37), 24.
8 T. R. Shrout and S. J. Zhang, *J. Electroceram.*, 2007, **19**, 113.
9 P. K. Panda, *J. Mater. Sci.*, 2009, **44**, 5049.
10 J. Roedel, W. Jo, K. T. P. Seifert, E.-M. Anton, T. Granzow and D. Damjanovic, *J. Am. Ceram. Soc.*, 2009, **92**, 1153.
11 X. H. Du, J. H. Zheng, U. Belegundu and K. Uchino, *Appl. Phys. Lett.*, 1998, **72**, 2421.
12 T. R. Shrout, Z. P. Chang, N. C. Kim and S. Markgraf, *Ferroelectr., Lett. Sect.*, 1990, **12**, 63.

13 H. Nagata, M. Yoshida, Y. Makiuchi and T. Takenaka, *Jpn. J. Appl. Phys.*, 2003, **42**, 7401.
14 L. Bellaiche and D. Vanderbilt, *Phys. Rev. Lett.*, 1999, **83**, 1347.
15 S. Wada, S. Suzuki, T. Noma, T. Suzuki, M. Osada, M. Kakihana, S. E. Park, L. E. Cross and T. R. Shrout, *Jpn. J. Appl. Phys.*, 1999, **38**, 5505.
16 D. Damjanovic, *J. Am. Ceram. Soc.*, 2005, **88**, 2663.
17 R. Ahluwalia, T. Lookman, A. Saxena and W. W. Cao, *Phys. Rev. B: Condens. Matter Mater. Phys.*, 2005, **72**, 014112.
18 L. Bellaiche, A. Garcia and D. Vanderbilt, *Phys. Rev. Lett.*, 2000, **84**, 5427.
19 B. Noheda, D. E. Cox, G. Shirane, S. E. Park, L. E. Cross and Z. Zhong, *Phys. Rev. Lett.*, 2001, **86**, 3891.
20 H. Birol, D. Damjanovic and N. Setter, *J. Eur. Ceram. Soc.*, 2006, **26**, 861.
21 B. Malic, J. Bernard, J. Holc, D. Jenko and M. Kosec, *J. Eur. Ceram. Soc.*, 2005, **25**, 2707.
22 Y. P. Guo, K. Kakimoto and H. Ohsato, *Mater. Lett.*, 2005, **59**, 241.
23 Y. Hiruma, R. Aoyagi, H. Nagata and T. Takenaka, *Jpn. J. Appl. Phys.*, 2004, **43**, 7556.
24 W. Chen, Y. M. Li, Q. Xu and J. Zhou, *J. Electroceram.*, 2005, **15**, 229.
25 W. Liu and X. Ren, *Phys. Rev. Lett.*, 2009, **103**, 257602.
26 S. Su, R. Zuo, S. Lu, Z. Xu, X. Wang and L. Li, *Curr. Appl. Phys.*, 2011, **11**, S120.
27 Y. Zeng, Y. Zheng, X. Tu, Z. Lu and E. Shi, *J. Cryst. Growth*, 2012, **343**, 17.
28 M. Wang, R. Zuo, S. Qi and L. Liu, *J. Mater. Sci.: Mater. Electron.*, 2011, **23**, 753.
29 H. Bao, C. Zhou, D. Xue, J. Gao and X. Ren, *J. Phys. D: Appl. Phys.*, 2010, **43**, 465401.
30 S. Bai, Q. Xu, L. Gu, F. Ma, Y. Qin and Z. L. Wang, *Nano Energy*, 2012, **1**, 789.
31 R. Agrawal, B. Peng and H. D. Espinosa, *Nano Lett.*, 2009, **9**, 4177.
32 Y. Qin, X. Wang and Z. L. Wang, *Nature*, 2008, **451**, 809.
33 A. V. Desai and M. A. Haque, *Sens. Actuators, A*, 2007, **134**, 169.
34 W. Wu, S. Bai, M. Yuan, Y. Qin, Z. L. Wang and T. Jing, *ACS Nano*, 2012, **6**, 6231.
35 L. Gu, N. Cui, L. Cheng, Q. Xu, S. Bai, M. Yuan, W. Wu, J. Liu, Y. Zhao, F. Ma, Y. Qin and Z. L. Wang, *Nano Lett.*, 2013, **13**, 91.
36 S. Xu, Y. Qin, C. Xu, Y. Wei, R. Yang and Z. L. Wang, *Nat. Nanotechnol.*, 2010, **5**, 366.
37 P. M. Rørvik, T. Grande and M.-A. Einarsrud, *Adv. Mater.*, 2011, **23**, 4007.
38 B. Li, J. E. Blendell, K. J. Bowman and M. Hoffmann, *J. Am. Ceram. Soc.*, 2011, **94**, 3192.
39 V. S. Puli, A. Kumar, D. B. Chrisey, M. Tomozawa, J. F. Scott and R. S. Katiyar, *J. Phys. D: Appl. Phys.*, 2011, **44**, 395403.
40 P. Hansen, D. Hennings and H. Schreinemacher, *J. Am. Ceram. Soc.*, 1998, **81**, 1369.
41 Y. Kobayashi, O. J. Hernandez, T. Sakaguchi, T. Yajima, T. Roisnel, Y. Tsujimoto, M. Morita, Y. Noda, Y. Mogami, A. Kitada, M. Ohkura, S. Hosokawa, Z. F. Li, K. Hayashi, Y. Kusano, J. E. Kim, N. Tsuji, A. Fujiwara, Y. Matsushita, K. Yoshimura, K. Takegoshi, M. Inoue, M. Takano and H. Kageyama, *Nat. Mater.*, 2012, **11**, 507.
42 X. Chen, S. Y. Xu, N. Yao and Y. Shi, *Nano Lett.*, 2010, **10**, 2133.

